Journal of Power Sources 185 (2008) 519–525

Contents lists available at ScienceDirect

Journal of Power Sources

journal homepage: www.elsevier.com/locate/jpowsour

Electrochemical performances of nanostructured Ni_3P–Ni films electrodeposited on nickel foam substrate

J.Y. Xiang[a], J.P. Tu[a,*], X.L. Wang[a], X.H. Huang[a], Y.F. Yuan[b], X.H. Xia[a], Z.Y. Zeng[a]

[a] Department of Materials Science and Engineering, Zhejiang University, Hangzhou 310027, China
[b] School of Mechanical and Automation Control, Zhejiang Sci-Tech University, Hangzhou 310032, China

ARTICLE INFO

Article history:
Received 8 April 2008
Received in revised form 17 June 2008
Accepted 23 June 2008
Available online 10 July 2008

Keywords:
Ni_3P–Ni film
Electrodeposition
Anode
Lithium ion battery

ABSTRACT

Ni_3P–Ni films were deposited on nickel foam substrates by electrodeposition in an aqueous solution. The structure and morphology of the electrodeposited films were characterized using X-ray diffraction (XRD) and scanning electron microscope (SEM). The annealed electrodeposited films consisted of tetragonal structured Ni_3P and cubic metal Ni. As anode for lithium ion batteries, the electrochemical properties of the Ni_3P–Ni films were investigated by cyclic voltammetry (CV), electrochemical impedance spectrum (EIS) and galvanostatic charge–discharge tests. The electrodeposition time had a significant effect on the electrochemical performances of the films. The Ni_3P–Ni film electrodeposited for 20 min delivered the initial discharge capacity of 890 mAh g^{-1}. Although the irreversible capacity at the first cycle was relative large, the Ni_3P–Ni film exhibited good cycling stability and its discharging capacity still maintained 340 mAh g^{-1} after 40 cycles.

1. Introduction

In the field of lithium ion batteries, most research efforts have been devoted to improving the efficiency of anode conversion reaction. A promising approach is that of reducing the polarization and enhancing the kinetics in electrode reactions [1–4]. Phosphides have attracted much attention in recent years due to the low polarization and good cycling stability. Gillot et al. [4] reported that the charge–discharge polarization ΔV of fluorides, oxides, sulfides and phosphides as anodes decreased from metal-fluorides (M-F) to metal-phosphides (M-P). Phosphides have the lowest polarization ΔV (about 0.4 V), and reacted with Li over the lowest and narrowest potential range. For instance, FeP_2 [5], CoP_3 [6,7], Cu_3P [8,9] and Ni_3P [10] reacted with Li at an average voltage of 1 V and delivered flat charge and discharge curves separated by about 0.4–0.5 V. In addition, the stable cycling performance is also essential for promising anode material. Some attempts have been made to improve the capacity retention of the phosphides. Zhang et al. adopted a high-energy ball-milling method to prepare CoP_x (CoP_3 + CoP) which could exhibit a reversible capacity of 533 mAh g^{-1} [11]. Bichat et al. [12] found that the micro-sized Cu_3P powders obtained by a solvothermal method have the better cycling performance than other Cu_3P powders prepared by ball milling, ceramic or spray method. Gillot et al. [4] reported that monoclinic NiP_2 obtained by a high-temperature ceramic route could reversibly take 5 Li^+ per formula unit.

Compared with the ball milling, solvothermal, and high-temperature ceramic process, electrodeposition is a simple, low-cost method to prepare thin films for anode materials,

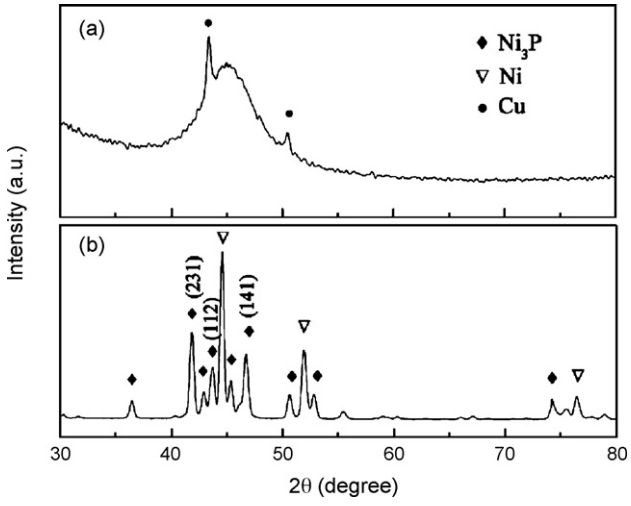

Fig. 1. XRD patterns of (a) precursor film and (b) annealed film.

* Corresponding author. Tel.: +86 571 87952573; fax: +86 571 87952856.
E-mail address: tujp@zju.edu.cn (J.P. Tu).

0378-7753/$ – see front matter © 2008 Elsevier B.V. All rights reserved.
doi:10.1016/j.jpowsour.2008.06.084

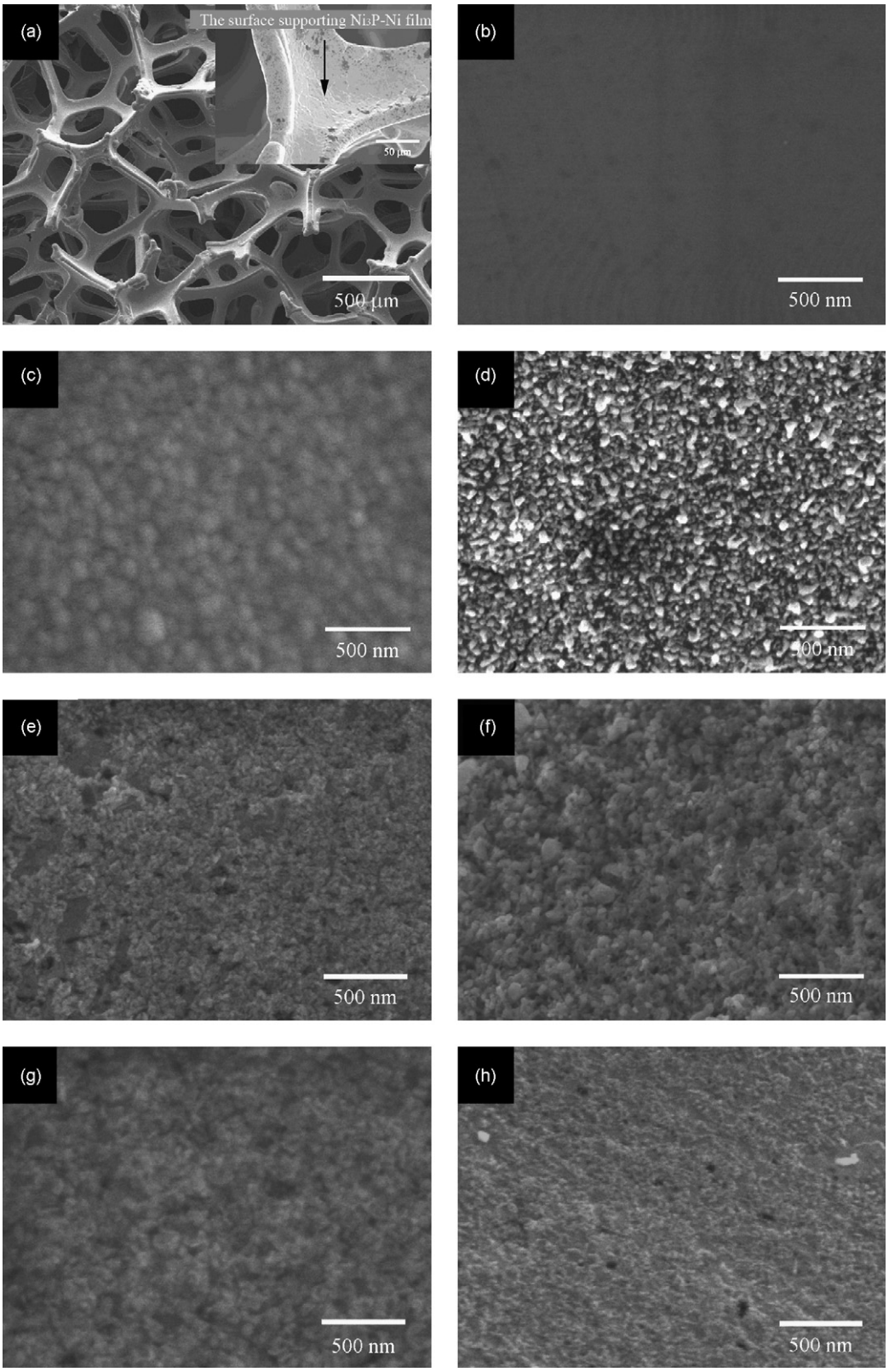

Fig. 2. SEM images of (a), (b) pure nickel foam, (c) precursor film, and (d)–(h) annealed Ni_3P–Ni films with electrodeposition time of 10–30 min.

which usually exhibit a long cycling life [13–15]. Furthermore, nickel–phosphorous alloys prepared by electrodeposition have been already used as protective coatings against corrosion [16,17]. However, the electrodeposited nickel phosphides were seldom investigated as anode for lithium ion batteries. Cruz et al. [10] reported that Ni_3P film electrodeposited on stainless steel had better capacity retention than bulk Ni_3P, but exhibited a low reversible capacity less than 100 mAh g^{-1} after a few cycles. In this work,

Ni_3P–Ni films were electrodeposited on nickel foam as anode for lithium ion batteries. The porous nickel foam used as current collector could increase the contact area between active material and electrolyte, which resulted in good electrode reactivity. The structure, surface morphology and electrochemical performances of the as-prepared Ni_3P–Ni films were investigated in details.

2. Experimental

The Ni_3P–Ni films were electrodeposited in a three-electrode system with nickel foam substrate (12 mm in diameter) as the working electrode, a Pt foil as the counter electrode and a saturated calomel electrode (SCE) as the reference electrode. The bath compositions contained 0.6 M $NiSO_4{\cdot}6H_2O$, 0.2 M $NiCl_2{\cdot}6H_2O$, 0.8 M H_3BO_3 and 0.6 M $NaH_2PO_4{\cdot}H_2O$. The electrodeposition was conducted at 75 °C and at a current density of 120 mA cm^{-2}, and the duration time was 10 min, 15 min, 20 min, 25 min and 30 min, respectively. After the electrodeposition, the films were annealed at 500 °C for 1 h under the flowing argon atmosphere and cooled with furnace to room temperature.

The structure and surface morphology of the Ni_3P–Ni films were characterized by X-ray diffraction (XRD, Philips PC-APD with Cu Kα radiation) and field emission scanning electron microscopy (FESEM, Hitachi S-4700), respectively.

Electrochemical performances of the Ni_3P–Ni films were investigated with a two-electrode coin-type cell (CR 2025). The as-prepared Ni_3P–Ni film on foam nickel was used as the working electrode, the metallic lithium foil as both the reference and counter electrodes, 1 M LiPF6 in ethylene carbonate (EC)–dimethyl carbonate (DME) (1:1 in volume) as the electrolyte solution, and a polypropylene (PP) microporous film (Cellgard 2300) as the separator. The cells were assembled in an Ar-filled glove box. The galvanostatic charge–discharge tests were conducted on a BS-9390 battery program-control test system at different current densities in the voltage range of 0.02–3.0 V (versus Li/Li^+) at room temperature (25 ± 1 °C). Cyclic voltammetry (CV) and electrochemical impedance spectrum (EIS) were performed on a CHI660C electrochemical workstation.

3. Results and discussion

Fig. 1 shows the XRD patterns of the electrodeposited precursor film and annealed film with the electrodeposition time of 10 min. Pure copper foil was used as the substrate here in order to avoid confusion in later analysis. Besides the peaks of Cu substrate, there is only a wide diffraction peak in the precursor film, which indicates that the precursor film is amorphous as shown in Fig. 1a. After annealed at 500 °C for 1 h, the film exhibits excellent crystallization (Fig. 1b). All the diffraction peaks can be indexed to two phases, one is tetragonal structured Ni_3P of *I4* space group ($a = b = 8.952$ Å, $c = 4.388$ Å), and the other is cubic metal nickel of *Fm3m* space group. It can be concluded that the annealed electrodeposited film consists of Ni_3P and Ni. The XRD patterns of other

Table 1
Mass of Ni_3P–Ni films on nickel foam with different electrodeposition times

Electrodeposition time (min)	Mass of Ni_3P–Ni film (mg cm^{-2})	
	Before annealing	After annealing
10	2.33	2.17
15	3.15	2.93
20	3.91	3.78
25	4.38	4.22
30	4.72	4.50

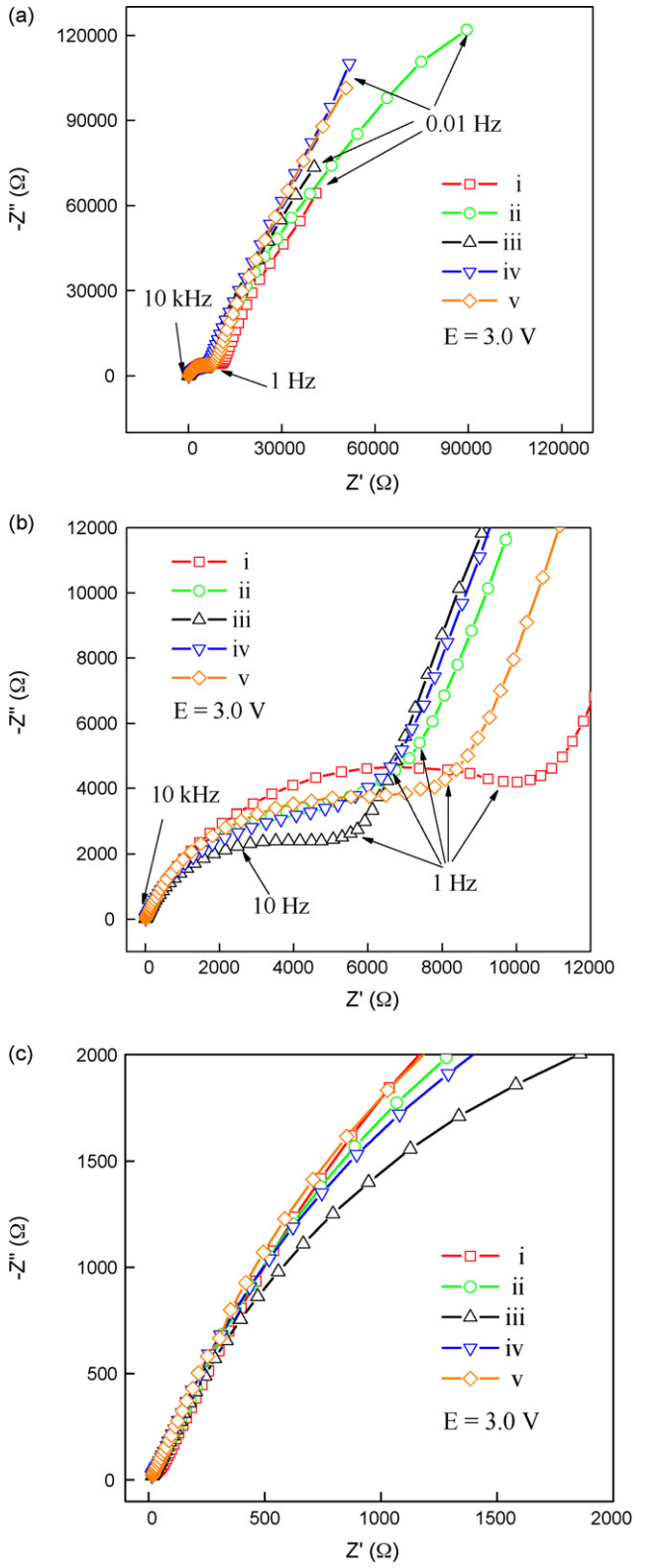

Fig. 3. AC impedance spectra of Ni_3P–Ni films with different electrodeposition time (i, 10 min; ii, 15 min; iii, 20 min; iv, 25 min; v, 30 min): (a) spectrum in total frequency range, (b) enlargement in high–medium frequency range, (c) enlargement in high frequency range.

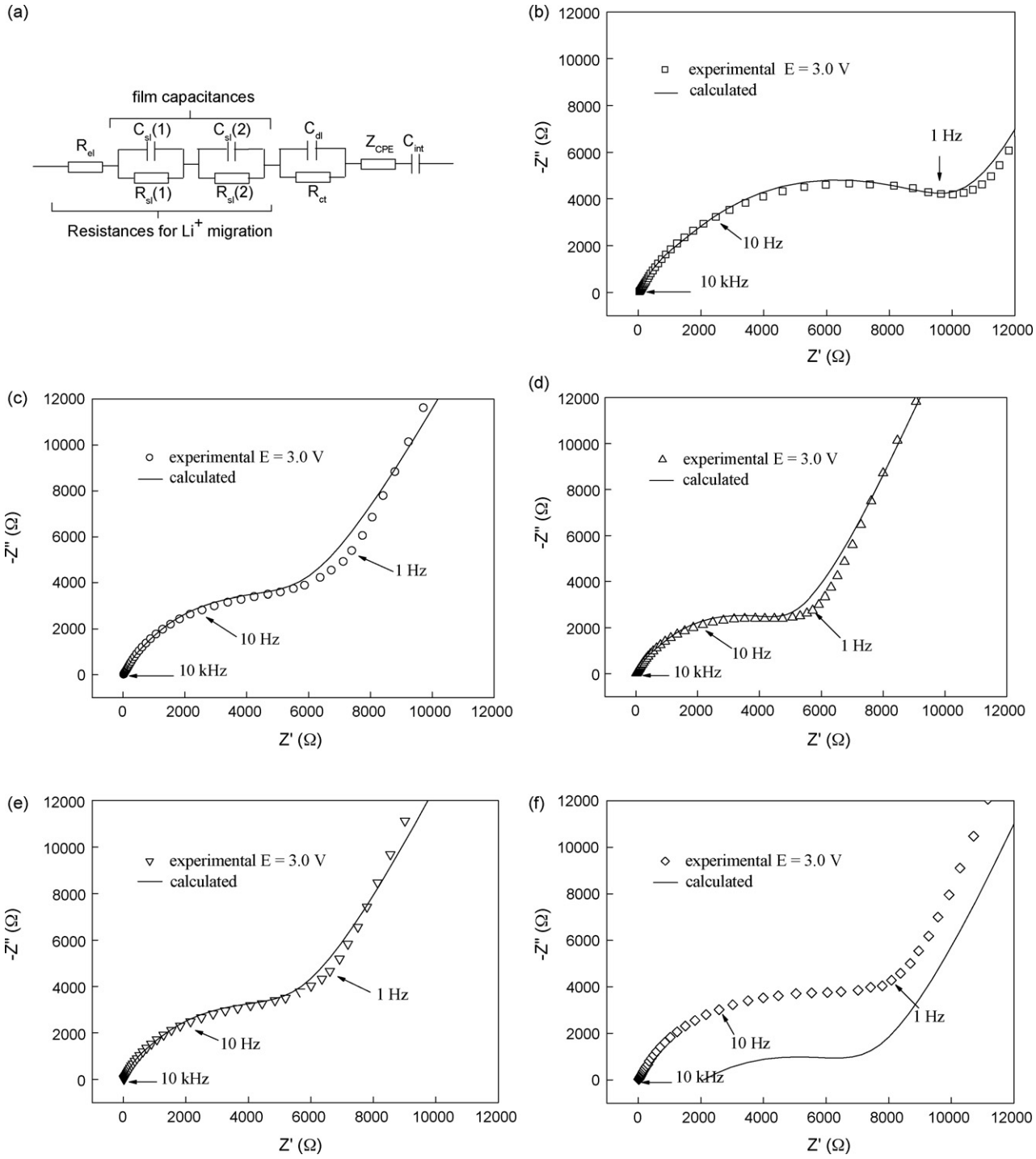

Fig. 4. (a) The model designed to simulate Nyquist plot of Ni_3P–Ni film, (b)–(f) fitting of the experimental Nyquist plot of the film with electrodeposition time of 10–30 min and that calculated using the model.

precursor films and annealed films with the electrodeposition time of 15–30 min are similar to Fig. 1a and b.

Fig. 2 shows the SEM images of pure nickel foam and the as-prepared Ni_3P–Ni films. Nickel foam substrate is the netlike frames, as shown in Fig. 2a. Its porous structure increases the contact area between the bath solution and Ni substrate, which results in an increase in mass of the electrodeposited Ni_3P–Ni film loading on Ni substrate. In addition, the porous structure may lead to a larger electrode/electrolyte contact area, which is beneficial to get higher specific capacity and better cycling stability. As shown in Fig. 2b, the surface of Ni foam is relatively smooth before electrodeposition. Fig. 2c displays the surface morphology of electrodeposited precursor film. The surface of precursor film is rough and composed of amorphous spherical particles with about 100–200 nm in diameters. After annealed at 500 °C for 1 h, the morphologies of the Ni_3P–Ni films change significantly as shown in Fig. 2d–f. The particles exhibit distinct crystal morphology and the particle size is about 50–100 nm. The morphology and size distribution of all the electrodeposited Ni_3P–Ni films are very homogeneous, and exceed those of anode materials prepared by ball milling,

solvothermal or high-temperature ceramic process. What is more, nanostructured Ni_3P–Ni films provide not only shorter diffusion path both for electrons and lithium ions, but also larger electrode-electrolyte contact area. Accordingly, nanostructured Ni_3P–Ni films exhibit better electrochemical properties than conventional materials. Similar phenomena have been shown in some early papers [14,18].

Table 1 lists the mass of Ni_3P–Ni films electrodeposited on nickel foam substrates for 10 min to 30 min. The loading speed is quick at first, and subsequently slow, which indicates that Ni_3P–Ni films grow adequately and cover on the nickel foam. As the electrodeposition time increases, the electrodeposited Ni_3P–Ni film becomes thicker.

Fig. 3 shows the impedance plots of the Ni_3P–Ni films with electrodeposition time of 10–30 min from 0.01 Hz to 10 KHz. Nyquist plot in the very high frequency range is nearly a line, and presents only one semicircle in high–medium frequency range. In order to clearly illuminate the AC impedance spectra of Ni_3P–Ni film, a model has been built in Fig. 4a. R_{el} indicates the solution resistance; $R_{sl}(i)$ and $C_{sl}(i)$ $(i = 1, 2)$ stands for the migration of lithium ions and capacity of the surface layer, respectively; R_{dl} and C_{dl} designates the related charge-transfer resistance and double-layer capacitance; and in the low frequency, Z_{CPE} is the semi-infinite Li^+ diffusion impedance, C_{int} stands for the Li^+ intercalation capacitance. Fig. 4b–f presents the excellent fitness between the simulated curve and the experimental Nyquist plots, which indicates the accuracy of the simulated model.

Since the AC impedance spectra were measured at an opening circular voltage (OCV) of 3.0 V after the first charge, almost all lithium ions were de-intercalated from Ni_3P–Ni film. So the Nyquist plots represent the capacitive effect of the fresh cell instead of the Wargurg impedance of discharge state at low frequency [19]. Hence, the semicircle in high–medium frequency is mainly induced from the intrinsic electronic resistance and contact resistance of the electrode rather than from the charge-transfer effect after the electrode is fully charged [19,20].

The contacts mentioned here include Ni_3P/Ni foam collector, Ni_3P/Ni_3P and Ni_3P/Ni particles among the film. Since the contact between Ni_3P film and Ni foam collector does not change with different electrodeposition time, the diameter of semicircle in high–medium frequency is mainly influenced by the contact of Ni_3P/Ni_3P and Ni_3P/Ni particles. Better contact of each particle in the film can lead to lower polarization and better cycling stability at higher rate. In this work, the Ni_3P–Ni film with electrodeposition time of 20 min has the least semicircle diameter in high–medium frequency. It is believed that the appropriate electrodeposition time is 20 min.

Fig. 5 displays the typical charge–discharge curves of Ni_3P–Ni film electrodeposited for 20 min. The initial discharge capacity is as high as 890 mAh g^{-1}. After the first cycle, the discharge capacity of Ni_3P–Ni film is relatively stable and maintains about 400 mAh g^{-1}. Even after 40 cycles, the Ni_3P–Ni film can still deliver the capacity of 340 mAh g^{-1}. For many metal phosphides, the mechanism of the electrochemical reactions is that the phosphides react with Li, and then change into some metal and Li_3P [10,21,22]. Accordingly, the electrode reaction of Ni_3P may be expressed as follows:

$$Ni_3P + (3 - 3x)Li \Leftrightarrow (3 - 3x)Ni + (1 - x)Li_3P + x''Ni_3P''_{unreacted} \quad (1)$$

If $x = 0$, the reaction proceeds completely, the cell can insert 3 Li^+ per unit of Ni_3P, and the reversible capacity of Ni_3P can reach to 400 mAh g^{-1}. However, the Ni_3P–Ni film electrodeposited for 20 min delivered an initial discharge capacity of 890 mAh g^{-1}, which was much higher than the theoretical value (400 mAh g^{-1}) of Ni_3P. The extra capacity could be attributed to the formation of the SEI film on the nanoparticles during the discharge process [23]. The

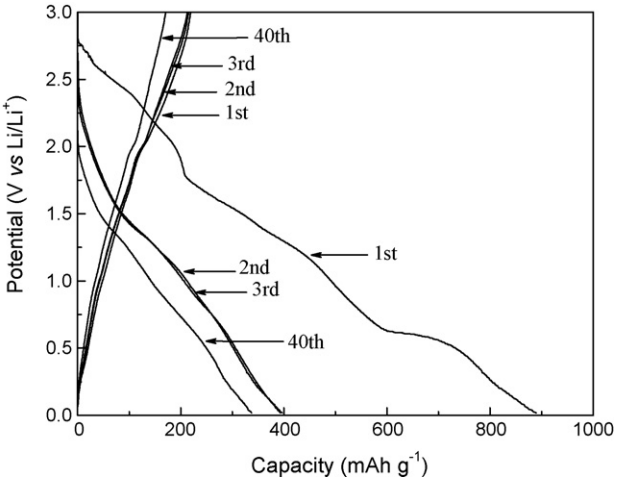

Fig. 5. The discharge–charge curves of Ni_3P–Ni film electrodeposited for 20 min ranging from 0.2 V to 3.0 V (1st, 2nd, 3rd and 40th).

discharge capacity can maintain about 400 mAh g^{-1} in the remaining cycles. According to the calculation, the cell inserts 2.6–3.0 Li^+ per unit of Ni_3P and $x = 0.4$–0, which means that the Ni_3P–Ni film reacts almost completely during the charge–discharge cycling.

In the discharge process of electrodeposited Ni_3P–Ni film, besides a broad plateau corresponding to reaction (1) at the potential from 1.5 V to 0.8 V [10] and a plateau corresponding to the formation of SEI film under 0.5 V [23], there is a small but notable voltage plateau located near 2.0 V in the discharge curve. It indicates that a reaction may take place as the discharge gets down to 2.0 V. To determinate the reaction occurred near 2.0 V, ex situ XRD pattern of the film electrode at the potential of 2.0 V is measured as shown in Fig. 6. In this pattern, besides the peaks of Ni substrate, Li_3P, and unreacted Ni_3P, other peaks can be indexed to $Ni_{12}P_5$ which is tetragonal structured as Ni_3P, and with lattice constants $a = b = 8.646$ Å, $c = 5.070$ Å. Therefore, it can be concluded that an intermediate compound $Ni_{12}P_5$ is formed during the discharge process. Since the structure and lattice constants of $Ni_{12}P_5$ and Ni_3P are similar, the transformation between $Ni_{12}P_5$ and Ni_3P would not induce much internal stress.

Fig. 7 shows the morphology of Ni_3P–Ni film electrodeposited for 20 min after the 1st and 40th cycles. Comparing with Fig. 2f, although the particle size increases, the morphologies of Ni_3P–Ni

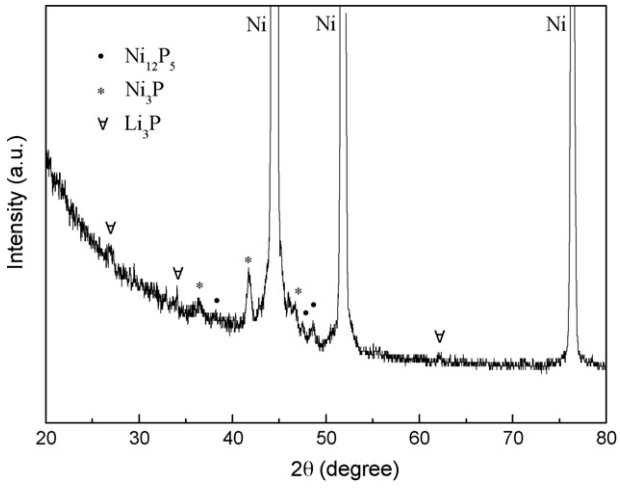

Fig. 6. Ex situ XRD pattern of Ni_3P–Ni film on nickel foam as the discharge gets down to 2.0 V.

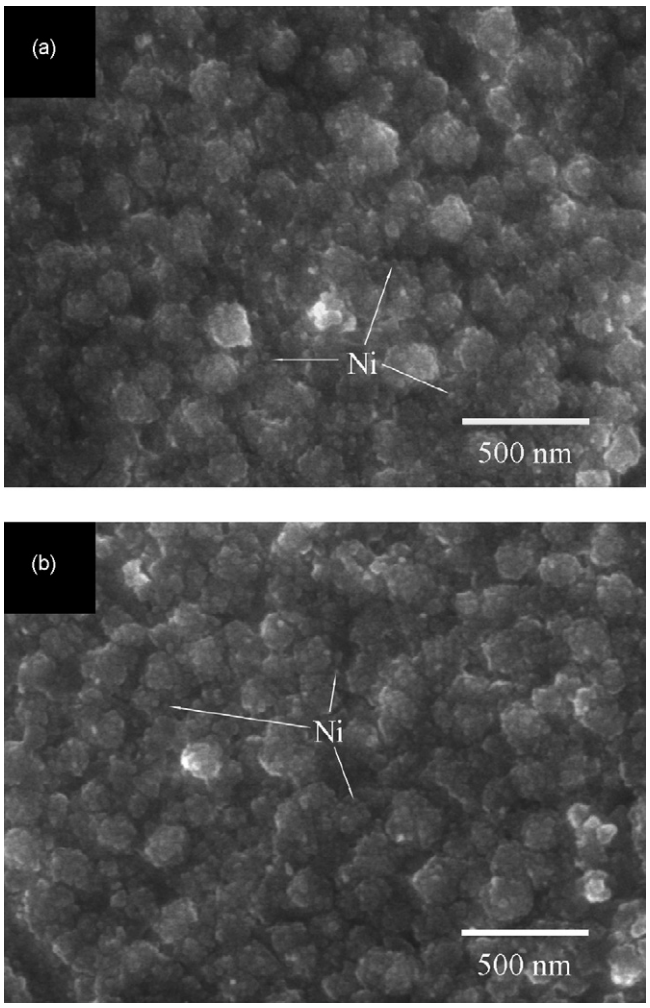

Fig. 7. SEM images of Ni_3P–Ni film electrodeposited for 20 min after the 1st and 40th cycles.

film after the 1st and 40th cycles do not change significantly, as shown in Fig. 7a and b. That is to say, the Ni_3P–Ni film has a good endurance against the stresses induced by volume expansion. The volume expansion generally results from the reversible transformation between Ni_3P and $Ni + Li_3P$. The morphology stability of the film can stabilize cycling performance of the electrode [24–26]. Furthermore, the nano-sized particles dispersed among the aggregated Ni_3P film is nickel, which will act as the catalyst to facilitate Li_3P decomposition (the converse reaction in Eq. (1)) to improve the electrochemical properties of the Ni_3P–Ni electrode.

Fig. 8 presents the first CV curves for Ni_3P–Ni films at a scan rate of 0.01 mV s^{-1} from 0 V to 3.0 V. The cathodic and anodic peaks are corresponding well with the discharge–charge plateaus in Fig. 5. Three distinct cathodic peaks are located at the potential of about 2.0 V, 1.3 V and 0.3 V, corresponding to the formation of the intermediate compound $Ni_{12}P_5$, reaction of Eq. (1) and electrolyte reduction and SEI formation [22], respectively.

The first CV curves of all the Ni_3P–Ni films are similar to each other, but the cathodic peaks corresponding to electrode reaction (1) slightly shift as the depositing time varies (Fig. 8b). Comparing with the cathodic peaks versus Li^+/Li of the different films, the peak of Ni_3P–Ni film electrodeposited for 20 min shifts to a relatively higher potential, while the peak of Ni_3P–Ni film electrodeposited for 10 min locates at the lowest position. Although the potentials of the cathodic peaks are different, the anodic peaks of the Ni_3P–Ni

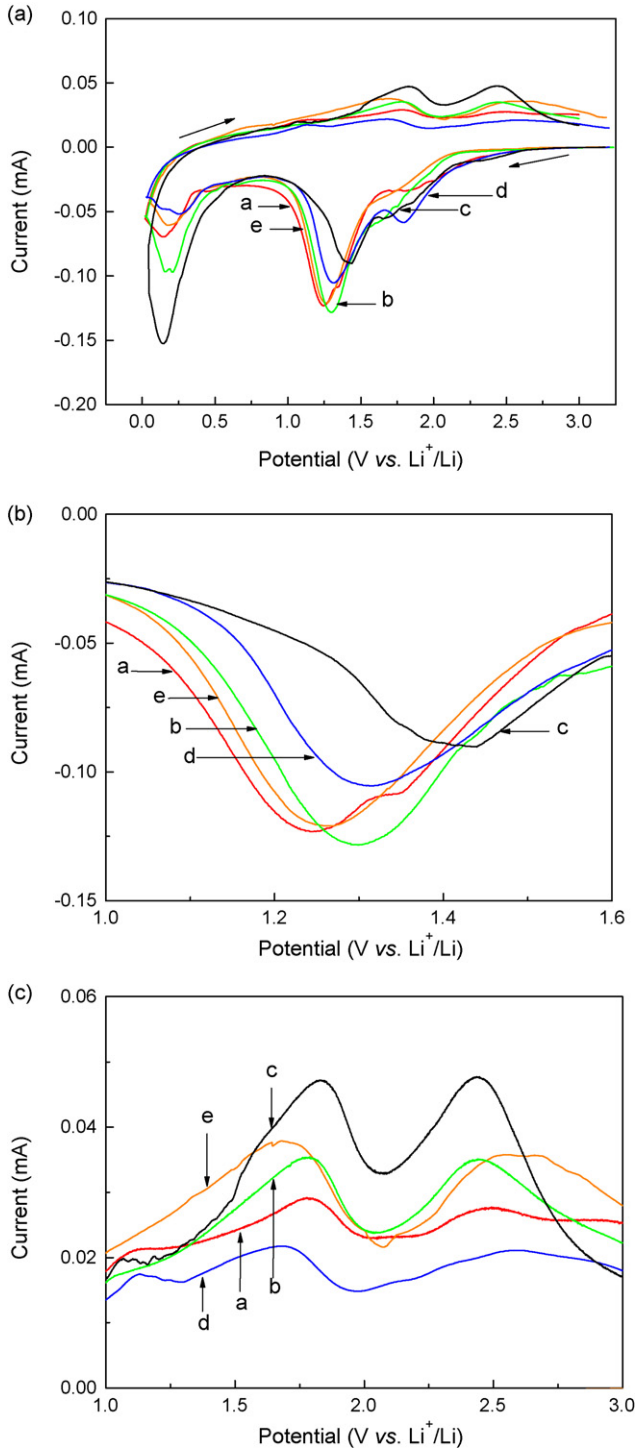

Fig. 8. The first cyclic voltammetry curves for Ni_3P–Ni films with different electrodeposition time (a, 10 min; b, 15 min; c, 20 min; d, 25 min; e, 30 min) at a scan rate of 0.1 mV s^{-1} from 0 V to 3.0 V.

films do not present any significant difference as shown in Fig. 8c. The interval between anodic and cathodic peaks is suggested as the polarization of the electrode. Therefore, Ni_3P–Ni film electrodeposited for 20 min shows the lowest polarization as indicated in Fig. 9.

The cycling performance (from the 2nd to 20th cycles) of Ni_3P–Ni films with different electrodeposition time is shown in Fig. 10. All the Ni_3P–Ni films exhibit good capacity retention at low rate and the discharge capacities are more than 340 mAh g^{-1}

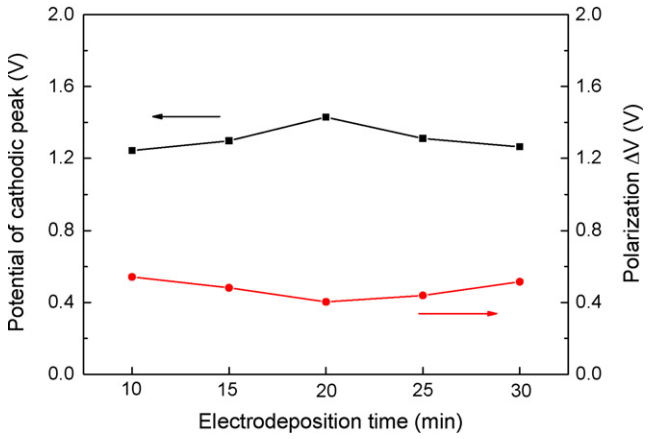

Fig. 9. Potential of cathodic reaction and polarization of Ni_3P–Ni films.

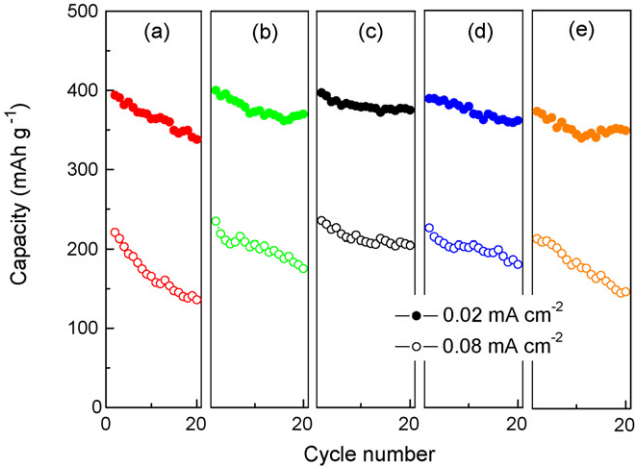

Fig. 10. Cycling performance of Ni_3P–Ni films with different electrodeposition times (a, 10 min; b, 15 min; c, 20 min; d, 25 min; e, 30 min).

after 20 cycles, which are 86–94% of the 2nd reversible capacity. However, as the rate increases, the discharge capacity declines a lot. For the Ni_3P–Ni films with electrodeposition time from 10 min to 30 min, the capacity retentions get down to 61%, 75%, 87%, 80% and 69% of the 2nd capacity after 20 cycles, respectively. The Ni_3P–Ni film electrodeposited for 20 min has the highest capacity retention. The good cycling performance of the Ni_3P–Ni film can be attributed to its small contact resistance and low polarization as discussed before.

4. Conclusions

Ni_3P–Ni films were successfully deposited on nickel foam substrates by electrodeposition in an aqueous solution. The films were amorphous before heat treatment, and changed into homogeneous crystalline after annealed at 500 °C for 1 h. The existence of Ni nanoparticles among Ni_3P film was supposed to facilitate the reversible reaction of the electrode. The electrodeposition time had a significant effect on the electrochemical performances of the films. In this work, the Ni_3P–Ni film electrodeposited for 20 min had the smallest contact resistance and lowest polarization. The Ni_3P–Ni film could exhibit an initial discharge capacity as high as 890 mAh g^{-1} under the discharge–charge current density of 0.02 mA cm^{-2}. Although there was a large irreversible capacity loss during the first cycle, the Ni_3P–Ni film delivered excellent cycling stability and still maintained 340 mAh g^{-1} even after 40 cycles.

References

[1] C.Q. Zhang, J.P. Tu, Y.F. Yuan, X.H. Huang, X.T. Chen, F. Mao, J. Electrochem. Soc. 154 (2007) A65–69.
[2] J. Xu, H.R. Thomas, R.W. Francis, K.R. Lum, J. Wang, B. Liang, J. Power Sources 177 (2008) 512–527.
[3] X.H. Huang, J.P. Tu, C.Q. Zhang, J.Y. Xiang, Electrochem. Commun. 9 (2007) 1180–1184.
[4] F. Gillot, S. Boyanov, L. Dupont, M.L. Doublet, M. Morcrette, L. Monconduit, Chem. Mater. 17 (2005) 6327–6337.
[5] D.C.C. Sliva, O. Crosnier, G. Ouvrard, J. Greedan, A. Safa-Safat, L. Nazar, Electrochem. Solid-State Lett. 6 (2003) A162–165.
[6] V. Pralong, D.C.S. Souza, K.T. Leung, L.F. Nazar, Electrochem. Commun. 4 (2005) 516–520.
[7] R. Alcantara, J.L. Tirado, J.C. Jumas, L. Monconduit, J. Olivier-Fourcade, J. Power Sources 109 (2002) 308–312.
[8] H. Pfeiffer, F. Tancret, M.P. Bichat, L. Monconduit, F. Faiver, T. Brousse, Electrochem. Commun. 6 (2004) 263–267.
[9] M.P. Bichat, T. Politova, H. Pfeiffer, F. Tancret, L. Monconduit, J.L. Pascal, T. Brousse, F. Favier, J. Power Sources 136 (2004) 80–87.
[10] M. Cruz, J. Morals, L. Sanchez, J. Santos-Pena, F. Martin, J. Power Sources 171 (2007) 870–878.
[11] Z.S. Zhang, J. Yang, Y. Nuli, B.F. Wang, J.Q. Xu, Solid State Ionics 176 (2005) 693–697.
[12] M.P. Bichat, T. Politova, J.L. Pascal, L. Dupont, M. Morcette, L. Monconduit, F. Favier, J. Electrochem. Soc. 151 (2004) 2074–2087.
[13] J. Morales, L. Sanchez, F. Martin, J.R. Ramos-Barrado, M. Sanchez, Electrochim. Acta 49 (2004) 4589–4597.
[14] J. Hassoun, S. Panero, B. Scrosati, J. Power Sources 160 (2006) 1336–1341.
[15] J.Y. Xiang, J.P. Tu, X.H. Huang, Y.Z. Yang, J. Solid State Electrochem. 12 (2008) 941–945.
[16] H.F. Ma, Z.B. Liu, F. Tian, H. Sun, J. Alloy Compd. 450 (2008) 348–351.
[17] C.S. Lin, C.Y. Lee, F.J. Chen, W.C. Li, J. Electrochem. Soc. 152 (2003) C370–375.
[18] H.C. Liu, S.K. Yen, J. Power Sources 166 (2007) 478–484.
[19] J.Y. Song, H.H. Lee, Y.Y. Wang, C.C. Wan, J. Power Sources 111 (2002) 255–267.
[20] Y. Zhang, X.G. Zhang, H.L. Zhang, Z.G. Zhao, F. Li, C. Liu, H.M. Cheng, Electrochim. Acta 51 (2006) 4994–5000.
[21] V. Pralong, D.C.S. Souza, K.T. Leung, L.F. Nazar, Electrochem. Commun. 4 (2002) 516–520.
[22] F. Gillot, M.-P. Bichat, F. Favier, M. Morcette, M.L. Doublet, L. Monconduit, Electrochim. Acta 49 (2004) 2325–2332.
[23] J.M. Tarascon, M. Morcrette, L. Dupont, Y. Chabre, C. Payen, D. Larcher, V. Pralong, J. Electrochem. Soc. 150 (2003) A732–741.
[24] G.X. Wang, J.H. Ahn, J. Yao, S. Bewlay, H.K. Liu, Electrochem. Commun. 6 (2004) 689–692.
[25] M. Noh, Y. Kwon, H. Lee, J. Cho, Y. Kim, M.G. Kim, Chem. Mater. 17 (2005) 1926–1929.
[26] C. Kim, M. Noh, M. Choi, J. Cho, B. Park, Chem. Mater. 17 (2005) 3297–3301.